KINEMATIC CHAIN STUDY OF THE ADJUSTABILITY OF A MONOLATERAL EXTERNAL FIXATOR

Sheng-Mou Hou, Jaw-Lin Wang, Chang-Yaw Soong, Tsung-Hung Lin, and Jinn Lin*

ABSTRACT

Adjustability of the external fixator reflects two important features–the range of allowable locations of pins and the ease of frame application. In this study, multilink open chain kinematic equations were developed to examine this adjustability of a monolateral external fixator. The entire bone-fixator system was simulated by a manipulator with four rigid links, two spherical joints, and one prismatic joint. Each of the links and joints was described by a 4×4 homogenous transformational matrix with either *X-Y-Z* or *Z-X-Z* Euler angle representation. The transformation equations were developed by concatenating these transformational matrices. Then the kinematic equations were solved by the least squares optimization method, and the numerical solutions were validated by geometrical solutions and mechanical experiments. The results showed solutions using *Z-X-Z* Euler angle representations were more reliable in predicting the reducibility of the malalignment and could be more conveniently used for direct kinematic study. Increasing the length of the central body, the offset of the telescoping joint, and the rotational range of ball joints and decreasing the pin length increased the adjustability. The adjustability reached its maximum as the initial offset of the telescoping joint reached a critical level. In conclusion, the adjustability of the external fixators was closely related to their designs. This study may assist manufacturers in the design of external fixators and help surgeons better understand the restraints of fixators and hence use such equipment more effectively.

Key Words: external fixator, adjustability, kinematic chain study.

I. INTRODUCTION

With the advent of modern technology and the use of powerful tools and speedy vehicles, more and more trauma caused by accidents threatens human life and health profoundly. Extremity fractures resulting from trauma should be treated by adequate reduction and rigid fixation. Healing of the fractures in anatomical position is the primary goal of fracture treatment (Christian, 1998). Furthermore, with sufficient fracture fixation, the patients can move immediately and start their joint exercise early. This may improve the patients' life quality and improve the functional recovery of their extremities. Generally speaking, fractures can be treated by either internal fixation or external fixation, depending on different fracture situations. The indications for use of external fixation include open fractures, multiple injuries, periarticular or intra-articular fractures, infected fractures, pelvic fractures, and children's fractures (Behrens and Searls, 1986; Bone *et al.*, 1993; Davis *et al.*, 1995; Nepola, 1996; Thakur, 1997). External fixation has the advantages of little tissue trauma and little blood loss. Also, because of minimal metallic implants in the contaminated wound, hardware-related infection can be avoided. Conventional multiplanar Hoffman external fixators comprised of multiple rigid rods and connecting joints have the disadvantages of bulkiness and inconvenience for patients and these

*Corresponding author. (Tel: 886-2-23123456 ext 5278; Fax: 886-2-23224112; Email:jin@ntumc.org)

S. M. Hou and J. Lin are with the Department of Orthopedic Surgery, National Taiwan University Hospital, Taipei, Taiwan 100, R.O.C.

J. L. Wang and C. Y. Soong are with the Department of Biomedical Engineering, National Taiwan University, Taipei, Taiwan 100, R.O.C.

T. H. Lin is with the Department of Mechanical Engineering, National Taiwan University of Science and Technology, Taipei, Taiwan 106, R.O.C.

devices can only be used to fix fractures statically. In the 1970s, a quick- and easy-to-use device, the dynamic axial fixator, was developed to overcome the disadvantages of the conventional Hoffman fixator (Nepola, 1996). This monolateral, uniplanar bar-type fixator with its telescoping body has the further advantage of dynamization to facilitate fracture union and lengthen the extremities. In addition, it has sufficient stability for lower-extremity fractures and can improve patients' daily functions, such as walking, squatting, or even sitting with legs crossed (Thakur, 1997). Although the structural stiffness of external fixators has been thoroughly investigated (Behrens et al., 1983; Briggs and Chao, 1982; Caja *et al.*, 1995; Caja. *et al.*, 1994; Chao and Hein, 1988; Fischer, 1983; Kummer, 1992; Paley *et al.*, 1990), another important feature of the external fixator, the adjustability–i.e., its ability to allow for various positions or directions of the pins–has rarely been reported on. This adjustability is particularly important for monolateral external fixators with limited numbers of joints. Using fixators with restricted adjustability, the operators may have to repeatedly readjust the positions of the pins or fixator in order to achieve fracture reduction or fixator application. This adjustability of the external fixators has been studied by Kim *et al*. (2002) using multilink kinematic chain theory with *X*-*Y*-*Z* Euler angle representations on two external fixators with hinge joints or ball joints respectively. With the fixators applied in a neutral position, the reducibility of a certain amount of fracture displacement in different directions was analyzed. First, the necessary motion of each connecting joint was solved by reverse kinematics, and then the possible pathways of fracture reduction were investigated. However, their mathematical solutions and the reduction pathways were not verified. Additionally, the *X*-*Y*-*Z* Euler angle representations can describe the motion of external fixators with multiple hinge joints, but it is not ideal for external fixators with ball-and-socket joints, in which the direction of the joint movement is not along *X*, *Y* or *Z* axes. In the present study, another method with *Z*-*X*-*Z* Euler angle representations has been introduced, which can more distinctly describe the motion of ball-and-socket joints and consequently be more reliable in prediction of the adjustability of the external fixator. The numerical solutions of the kinematic equations based on multilink kinematic chain theory were verified with close form geometrical solutions and mechanical experiments.

II. MATERIALS AND METHODS

1. Configuration of the Fixator

The standard Orthofix axial external fixator (Orthofix SRL, Verona, Italy) is a monolateral device with a single frame body containing two pin clamps, a central body with a telescoping joint, and two ball-and-socket joints that connect the pin clamps and the central body (Fig. 1). The pin clamps have five premachined slots for varying numbers of half pins. The ball joint comprises a spherical ball on the pin clamp, an encasing collar, and a hemispherical bushing contained in the central body, which is compressed by an eccentric cam to lock the joint. The spherical ball joints have three degrees of freedom (DOFs), allowing a total of ±18.5°C angulation in all directions and an unlimited axial rotation. The central body is divided into two segments of unequal length, which are connected by a telescoping joint. The telescoping joint is a prismatic joint with one DOF, allowing a maximal offset of 40 mm along the axis of the central body. The fixator is adjustable through rotation of the ball joints and protrusion of the telescoping joint.

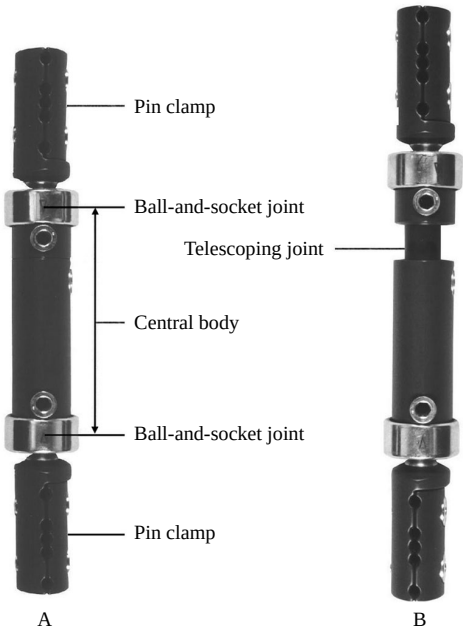

Fig. 1 Configuration of the Orthofix fixator. (A) The fixator without extension of telescoping joint. (B) The fixator with extension of telescoping joint.

2. Kinematic Chain Study

The long bone fragments were simulated by two unsymmetrical elliptical cylinders, which were connected to the external fixators by two groups of pins contained in two separate pin clamps (Fig. 2). The linkage of the bone fragments and the external fixator were simulated by an open-chain articulated manipulator with four rigid links of different shape and three intermediate joints. The inferior bone fragment was

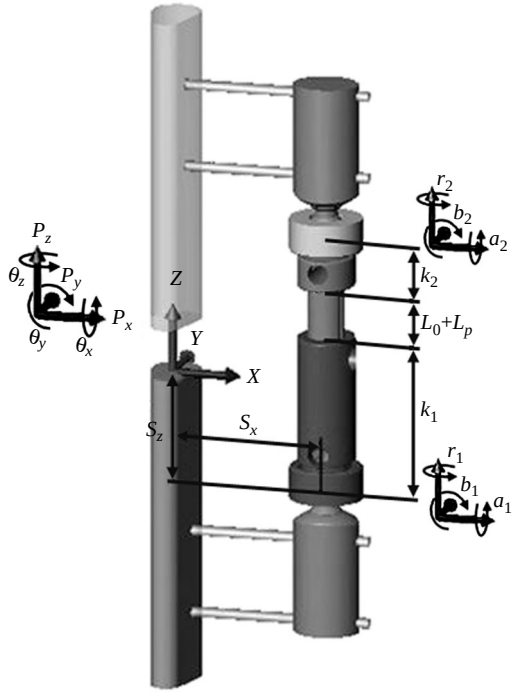

Fig. 2 Symbols used for the bone-fixator system. P_x, P_y, P_z, θ_x, θ_y, and θ_z are the positional vectors of bone fragments. S_x and S_z are the fixed parameters of Link 1 or 4 along the X- and Z-axes. L_0 is the initial offset of the telescoping joint. L_p is the protruded offset of the telescoping joint; a_1, b_1, r_1, a_2, b_2, and r_2 are the angulations of the ball joints.

the base and the superior bone fragment was the end-effecter. Link 1 included the inferior bone fragment, fixing pins, and the lower pin clamp. Link 2 was the central body between the inferior ball joint and the telescoping joint. Link 3 was the central body between the telescoping joint and the upper ball joint. Link 4 included the upper pin clamp, fixing pins, and the upper bone fragment. Joint 1 was the inferior ball joint connecting Link 1 and Link 2. Joint 2 was the telescoping joint connecting Link 2 and Link 3. Joint 3 was the superior ball joint connecting Link 3 and Link 4. For convenience in describing the direction of the translational and rotational vectors, the fixator was assumed to be applied to the lateral aspect of the left-side extremities. A global Cartesian frame was attached to the upper end of the inferior bone fragment with the X-axis directing laterally, Y-axis directing posteriorly, and Z-axis directing superiorly. Right-hand rule was used to define the direction of the rotational vectors. The spatial positioning of the upper bone fragment with respect to the global coordinate of the lower bone fragment has six DOFs and can be characterized mathematically by a 4×4 homogenous transformational matrix ($\boldsymbol{T}_{Bone}$). This $\boldsymbol{T}_{Bone}$ matrix is the product of the one translational matrix and three rotational matrices: $\boldsymbol{T}_{Bone}=\boldsymbol{T}_{(P_x,\ P_y,\ P_z)}\boldsymbol{T}_{(X,\ \theta_x)}\boldsymbol{T}_{(Y,\ \theta_y)}\boldsymbol{T}_{(Z,\ \theta_z)}$.

$$\boldsymbol{T}_{bone}=\begin{bmatrix} c\theta_y c\theta_z & -c\theta_y c\theta_z & s\theta_y & P_x \\ c\theta_x s\theta_z + s\theta_x s\theta_y c\theta_z & c\theta_x c\theta_z + s\theta_x s\theta_y c\theta_z & -s\theta_x c\theta_y & P_y \\ s\theta_x s\theta_z - c\theta_x s\theta_y c\theta_z & s\theta_x c\theta_z + c\theta_x s\theta_y s\theta_z & c\theta_x c\theta_y & P_z \\ 0 & 0 & 0 & 1 \end{bmatrix}$$

$$=\begin{bmatrix} 1 & 0 & 0 & P_x \\ 0 & 1 & 0 & P_y \\ 0 & 0 & 1 & P_z \\ 0 & 0 & 0 & 1 \end{bmatrix}\begin{bmatrix} 1 & 0 & 0 & 0 \\ 0 & c\theta_x & -s\theta_x & 0 \\ 0 & s\theta_x & c\theta_x & 0 \\ 0 & 0 & 0 & 1 \end{bmatrix}\begin{bmatrix} c\theta_y & 0 & s\theta_y & 0 \\ 0 & 1 & 0 & 0 \\ -s\theta_y & 0 & c\theta_y & 0 \\ 0 & 0 & 0 & 1 \end{bmatrix}\begin{bmatrix} c\theta_z & -s\theta_z & 0 & 0 \\ s\theta_z & c\theta_z & 0 & 0 \\ 0 & 0 & 1 & 0 \\ 0 & 0 & 0 & 1 \end{bmatrix}$$

Where $\boldsymbol{T}_{(P_x,\ P_y,\ P_z)}$ is a 4×4 homogenous translational matrix and $\boldsymbol{T}_{(X,\ \theta_x)}$, $\boldsymbol{T}_{(Y,\ \theta_y)}$, and $\boldsymbol{T}_{(Z,\ \theta_z)}$ are the rotational matrices. P_x, P_y, and P_z are the three translational vectors, and θ_x, θ_y, and θ_z are the three rotational vectors about the X-, Y-, and Z-axis, respectively. The letters c and s are shorthand for cosine and sine. Similarly, for the four links and three joints of the external fixator, 4×4 homogenous transformational matrices can also be given sequentially:

$$\boldsymbol{T}_{Link\ 1}=\begin{bmatrix} 1 & 0 & 0 & S_x \\ 0 & 1 & 0 & 0 \\ 0 & 0 & 1 & -S_z \\ 0 & 0 & 0 & 1 \end{bmatrix};$$

$$\boldsymbol{T}_{Joint\ 1}=\begin{bmatrix} 1 & 0 & 0 & 0 \\ 0 & ca_1 & -sa_1 & 0 \\ 0 & sa_1 & ca_1 & 0 \\ 0 & 0 & 0 & 1 \end{bmatrix}\begin{bmatrix} cb_1 & 0 & sb_1 & 0 \\ 0 & 1 & 0 & 0 \\ -sb_1 & 0 & cb_1 & 0 \\ 0 & 0 & 0 & 1 \end{bmatrix}$$

$$\cdot\begin{bmatrix} cr_1 & -sr_1 & 0 & 0 \\ sr_1 & cr_1 & 0 & 0 \\ 0 & 0 & 1 & 0 \\ 0 & 0 & 0 & 1 \end{bmatrix}$$

$$\boldsymbol{T}_{Link\ 2}=\begin{bmatrix} 1 & 0 & 0 & 0 \\ 0 & 1 & 0 & 0 \\ 0 & 0 & 1 & k_1 \\ 0 & 0 & 0 & 1 \end{bmatrix};$$

$$\boldsymbol{T}_{\textit{Joint 2}} = \begin{bmatrix} 1 & 0 & 0 & 0 \\ 0 & 1 & 0 & 0 \\ 0 & 0 & 1 & L_0 + L_p \\ 0 & 0 & 0 & 1 \end{bmatrix};$$

$$\boldsymbol{T}_{\textit{Link 3}} = \begin{bmatrix} 1 & 0 & 0 & 0 \\ 0 & 1 & 0 & 0 \\ 0 & 0 & 1 & k_2 \\ 0 & 0 & 0 & 1 \end{bmatrix}$$

$$\boldsymbol{T}_{\textit{Joint 3}} = \begin{bmatrix} 1 & 0 & 0 & 0 \\ 0 & ca_2 & -sa_2 & 0 \\ 0 & sa_2 & ca_2 & 0 \\ 0 & 0 & 0 & 1 \end{bmatrix} \begin{bmatrix} cb_2 & 0 & sb_2 & 0 \\ 0 & 1 & 0 & 0 \\ -sb_2 & 0 & cb_2 & 0 \\ 0 & 0 & 0 & 1 \end{bmatrix}$$

$$\cdot \begin{bmatrix} cr_2 & -sr_2 & 0 & 0 \\ sr_2 & cr_2 & 0 & 0 \\ 0 & 0 & 1 & 0 \\ 0 & 0 & 0 & 1 \end{bmatrix}$$

$$\boldsymbol{T}_{\textit{Link 4}} = \begin{bmatrix} 1 & 0 & 0 & -S_x \\ 0 & 1 & 0 & 0 \\ 0 & 0 & 1 & -S_z \\ 0 & 0 & 0 & 1 \end{bmatrix}$$

Where the symbols a_1, b_1, and r_1 represent the rotation of the lower ball joint, and a_2, b_2, and r_2 represent the rotation of the upper ball joint about the *X*-, *Y*-, and *Z*-axis, respectively. Here, the rotation of the ball joints is described by *X*-*Y*-*Z* Euler angle representations, in which the rotation is performed about an axis of a moving frame. (Craig, 1989) L_0 is the initial offset of the telescoping joint. L_p is the protruded offset of the telescoping joint. Fixed parameters of Link 1or Link 4 along the *X*-axis and *Z*-axis can be reduced to S_x and S_z. S_x (75 mm) is the distance between the bone fragment and the fixator, equivalent to the pin length. S_z is the vertical distance between the end of the bone fragment and the ball joint. In this study, the global coordinate about the position of the bone fragments at the upper end of the inferior bone fragment was assumed to be at the point corresponding to the middle of the fixator. Thus S_z is equal to $(k_1+k_2+L_0)/2$. The fixed parameters of Links 2 and 3 are k_1 (80 mm) and k_2 (20 mm). Then by concatenating the transformational matrices, we can develop the transformation equation: $\boldsymbol{T}_{\textit{Bone}} = \boldsymbol{T}_{\textit{Link 1}}\boldsymbol{T}_{\textit{Joint 1}}\boldsymbol{T}_{\textit{Link 2}}\boldsymbol{T}_{\textit{Joint 2}}\boldsymbol{T}_{\textit{Link 3}}\boldsymbol{T}_{\textit{Joint 3}}\boldsymbol{T}_{\textit{Link 4}}$. Equating the corresponding elements gives 12 kinematic equations; however, only six of them, three in rotation and three in translation, are independent (Appendices).

In addition to the *X*-*Y*-*Z* Euler angle representation, the sequence of rotation can also be described by *Z*-*X*-*Z* Euler angle representation (Chao and Hein, 1988):[8]

$$\boldsymbol{T}_{\textit{Joint 1}} = \begin{bmatrix} cr_1 & -sr_1 & 0 & 0 \\ sr_1 & cr_1 & 0 & 0 \\ 0 & 0 & 1 & 0 \\ 0 & 0 & 0 & 1 \end{bmatrix} \begin{bmatrix} 1 & 0 & 0 & 0 \\ 0 & ca_1 & -sa_1 & 0 \\ 0 & sa_1 & ca_1 & 0 \\ 0 & 0 & 0 & 1 \end{bmatrix}$$

$$\cdot \begin{bmatrix} cr_1' & -sr_1' & 0 & 0 \\ sr_1' & cr_1' & 0 & 0 \\ 0 & 0 & 1 & 0 \\ 0 & 0 & 0 & 1 \end{bmatrix}$$

$$\boldsymbol{T}_{\textit{Joint 3}} = \begin{bmatrix} cr_2 & -sr_2 & 0 & 0 \\ sr_2 & cr_2 & 0 & 0 \\ 0 & 0 & 1 & 0 \\ 0 & 0 & 0 & 1 \end{bmatrix} \begin{bmatrix} 1 & 0 & 0 & 0 \\ 0 & ca_2 & -sa_2 & 0 \\ 0 & sa_2 & ca_2 & 0 \\ 0 & 0 & 0 & 1 \end{bmatrix}$$

$$\cdot \begin{bmatrix} cr_2' & -sr_2' & 0 & 0 \\ sr_2' & cr_2' & 0 & 0 \\ 0 & 0 & 1 & 0 \\ 0 & 0 & 0 & 1 \end{bmatrix}$$

Where r_1 and r_2 are rotation of the ball joints about the *Z*-axis, a_1 and a_2 are rotation about the *X*-axis and r_1' and r_2' are rotation about the new *Z*-axis. To show the difference between these two representations, a special example of inverse kinematics was chosen: the original malalignment of the bone fragments was θ_z=-24.5° with a gap of P_z=-5 mm, and the external fixator was originally aligned in neutral position (a_1=b_1=r_1=a_2=b_2=r_2=L_0=0). Then the unknown joint variables were computed as the bone fragments were reduced. For direct kinematics, the adjustable range of the fixator as reflected by the relative positioning of bone fragments was computed on the basis of the given joint variables.

Because of the high nonlinearity of the transcendental kinematic equations, the iterative numerical solution done by the least squares optimization method based on different initial estimates was chosen (MATLAB 5.3, Mathworks, Natick, MA, USA). The initial estimates were randomly selected, starting at zero. If a solution could not be found, then another initial estimate was tried.

3. Geometrical Solution

The spatial geometry of the motion of an Orthofix external fixator can be decomposed to several planar geometric problems. The direct kinematics may be solved by trigonometric functions (MATLAB 5.3,

Table 1 Numerical solutions in *X-Y-Z* representation with no constraint under different initial estimates of r_1

Variable	*Solution 1		*Solution 2		*Solution 3		Solution 4		Solution 5	
	Initial Estimate	Solution	Initial Estimate	Solution	Initial Estimate	Solution	Initial Estimate	Solution	Initial Estimate	Solution
a_1 (°)	0	18.13	0	18.13	0	18.13	0	48.77	0	-72.07
b_1 (°)	0	-3.86	0	-3.86	0	-3.86	0	-16.48	0	-20.52
r_1 (°)	1	17.79	5	-51.43	-5	27.89	10	-161.71	-10	-152.6
L_p (mm)	0	0.19	0	0.19	0	0.19	0	4.00	0	-15.83
a_2 (°)	0	-16.27	0	-14.43	0	-14.71	0	-27.16	0	2.78
b_2 (°)	0	8.98	0	-11.73	0	11.39	0	-89.74	0	-116.04
r_2 (°)	0	-40.38	0	26.06	0	-49.20	0	16.69	0	-4.38

*Valid solution; mm = millimeter.

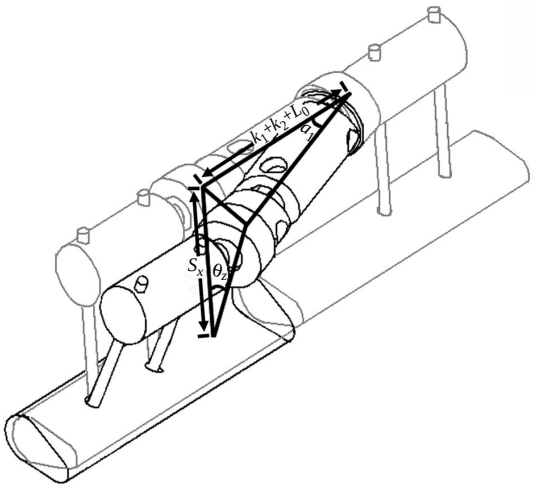

Fig. 3 Schematic diagram for the geometrical solution in direct kinematics. The configuration sketched with light gray lines represents the original position of the bone fragments and the fixator. The configuration sketched in black lines represents the new position after axial rotation of the bone fragment. The relationship between these two positions can be analyzed by the triangles formed by the heavy black lines. The symbols are defined in **Method** under *Kinematic chain study* section.

Mathworks, Natick, MA, USA), based on a right triangle and an isosceles triangle (Fig. 3). The inverse kinematics can be similarly solved. All the parameters were the same as those for the kinematic chain approach.

4. Mechanical Experiment

The range of the rotational motion of the bone fragments was studied by a mechanical experiment. The external fixator was applied to two straightly aligned cylindrical plastic tubes that were connected to a potentiometer (CPP-45, Midori America, Fullerton, CA, USA). The allowable range of axial rotation of the bone fragments was measured with different lengths of initial offset of the telescoping joint. The results were compared with those of the kinematic and geometrical solutions.

III. RESULTS

1. Kinematic Chain Study

Different initial estimates of r_1 and r_1' for *X-Y-Z* representation and *Z-X-Z* representation respectively were used to solve the kinematic equations, but some did not yield solutions. Five sets of computations with ultimate solutions are presented (Tables 1 and 2). The solutions of the rotation of the ball joints were reduced to between –180° and 180° in accordance with the periodic nature of the trigonometry. For inverse kinematics, because the entire multilink system had seven DOFs, outnumbering the independent equations, multiple solutions were obtained with different initial estimates. However, only some of the solutions were valid in terms of the limit of the joint motion. These solutions were characterized by the same protruded offset of the telescoping joint, but the rotations of the ball joints varied. This finding indicated that the final configurations of the fixator were not exactly the same, even though the bone fragments were reduced.

Subsequently, one of the rotational variables was constrained to reduce the redundancy. Thus, r_2 was set to zero in both *X-Y-Z* representation and *Z-X-Z* representation. Under these conditions, there was only one valid solution in the *X-Y-Z* representation: a_1=18.13, b_1=-3.86, r_1= 24.53, L_p=0.19, a_2=-18.09, b_2=-4.07, r_2=0, but there were still three in the *Z-X-Z* representation: r_1=167.75, a_1=-18.52, r_1'=180, L_p= 0.19, r_2=0, a_2=-18.52, r_2'=-12.25; r_1=-12.25, a_1= 18.52, r_1'= 0, L_p=0.19, r_2=0, a_2=-18.52, r_2'=-12.25 and r_1=167.75, a_1=-18.52, r_1'= 0, L_p=0.19, r_2=0, a_2=18.52, r_2'=167.75, when the same initial estimates as those in the situations without constraints were used. The malalignment of the bone fragments could be reduced

Table 2 Numerical solutions in *Z-X-Z* representation with no constraint under different initial estimates of r_1'

Variable	*Solution 1		*Solution 2		*Solution 3		*Solution 4		*Solution 5	
	Initial Estimate	Solution	Initial Estimate	Solution	Initial Estimate	Solution	Initial Estimate	Solution	Initial Estimate	Solution
r_1 (°)	0	167.75	0	-12.25	0	167.75	0	-12.25	0	167.75
a_1 (°)	0	-18.52	0	18.52	0	-18.52	0	18.52	0	-18.52
r_1' (°)	1	-67.19	5	-161.02	-5	45.46	10	138.91	-10	-107.39
L_p (mm)	0	0.19	0	0.19	0	0.19	0	0.19	0	0.19
r_2 (°)	0	67.19	0	161.02	0	-45.46	0	41.09	0	107.39
a_2 (°)	0	18.52	0	-18.52	0	18.52	0	18.52	0	18.52
r_2' (°)	0	167.75	0	-12.25	0	167.75	0	167.75	0	167.75

*Valid solution; mm = millimeter.

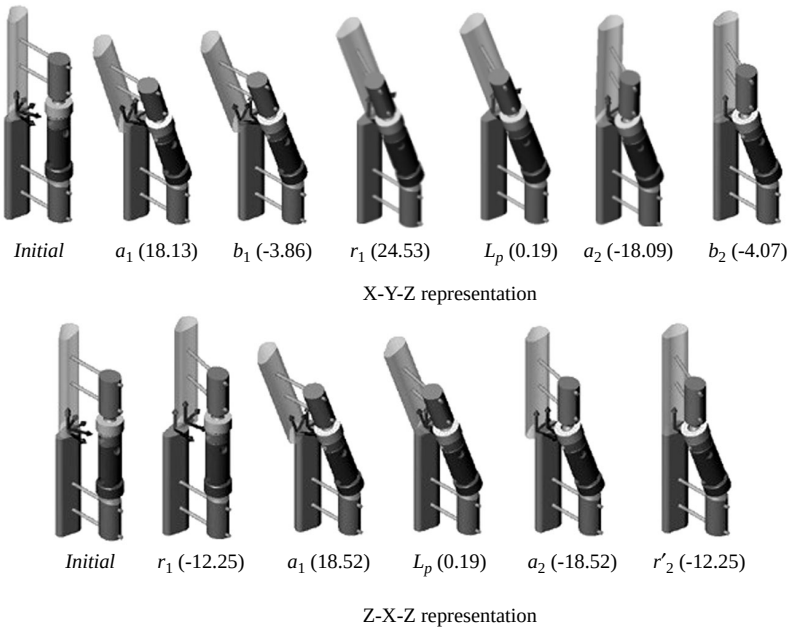

Fig. 4 The reduction pathways in *X-Y-Z* representation and *Z-X-Z* representation. In parentheses are the ranges of motion for each connecting joint. The symbols are defined in **Method** under *Kinematic chain study* section.

by sequential adjustment of each connecting joint (Fig. 4). For the example of inverse kinematics, *Z-X-Z* representation showed that the angulation (18.52°) of the ball joints was slightly beyond the joint limit (18.5°) of the fixators. This meant, strictly speaking, that the malalignment with a 24.5° axial rotation and a 5-mm gap was practically irreducible. An *X-Y-Z* representation might be unable to detect this irreducibility because a_1, b_1, and r_1 were all within the joint limit.

Besides better predictability of reducibility as compared with the *X-Y-Z* representation, the *Z-X-Z* representation had further advantage of expeditious use for direct kinematic study. The rotational range of the bone fragments (θ_z) could be computed straightforwardly by input of the initial offset of the telescoping joint (L_0) and the angles (a_1 or a_2) of the ball joints. As observed, the range of rotation increased as the initial offset of the telescoping joint increased (Fig. 5). With a pin length of 75 mm and joint angle of 18.5°, the maximal range of rotation was 34.45° as the initial offset of the telescoping joint reached the critical level of 32.77 mm. Beyond this level, because of the limitation of the telescoping joint, the range of the rotation inversely decreased as the initial offset of the telescoping joint increased (Fig. 5).

2. Geometrical Solution

For direct kinematics, the equations could be expressed as follows:

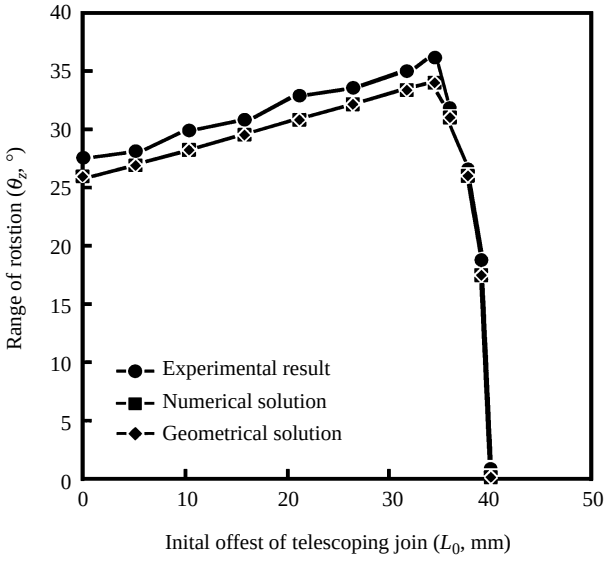

Fig. 5 Relationship between range of rotation (θ_z) and initial offset of the telescoping joint (L_0) in direct kinematics

With L_0<32.77 mm,

$$\theta_z=2\sin^{-1}[(k_1+k_2+L_0)\tan(a_1)/(2S_x)],$$

$$L_p=(k_1+k_2+L_0)[1/\cos(a_1)-1];$$

With L_0>32.77 mm,

$$\theta_z=2\sin^{-1}[(k_1+k_2+L_0)\tan(a_1)/(2S_x)],$$

$$a_1=\cos^{-1}[(k_1+k_2+L_0)/(k_1+k_2+40)],\ L_p=40-L_0.$$

For inverse kinematics, the equations were as follows:

$$a_1=a_2=\tan^{-1}[2S_x\sin(\theta_z/2)/(k_1+k_2+L_0-P_z)];$$

$$L_p=[2S_x\sin(\theta_z/2)/\sin(a_1)]-(k_1+k_2+L_0).$$

For both direct and inverse kinematic studies, the geometric solutions were almost completely the same as the numerical solutions (Fig. 5).

3. Mechanical Experiment

The measured range of rotation in the mechanical experiment was somewhat larger than in the two mathematical models, but in all three models the relation of range of motion to the initial offset of the telescoping joint was similar (Fig. 5).

IV. DISCUSSION

In external fixation of some complex fractures, the reduced fractures tend to redisplace because of inherent instability. Under these circumstances, external fixators can be attached with loosely connecting joints to fixing pins that are preinserted into the fracture fragments when the fractured limb is provisionally aligned. Then, right at the moment when the fracture is precisely reduced, the connecting joints are fastened to fix the fracture rigidly. Good adjustability of the external fixator can facilitate the above-described procedures, and it allows further readjustment after the frame is completed. Moreover, in open fractures with large and irregular soft tissue defects, good adjustability allows placement of fixing pins away from the fracture hematoma and the injury zone to prevent pin tract infection (Nepola, 1996). Good adjustability can also allow application of the pins in different planes to avoid neurovascular or musculotendinous injuries (Thakur, 1997).

The kinematics of the mechanical manipulator, which is widely used in manufacturing processes, can be applied to an investigation of the complex spatial motion of external fixators, whose structure is similar to the manipulator's. In this study, each of the links and joints of the external fixator was described by a 4×4 homogenous transformational matrix. Kinematic studies could then be conducted by concatenating these transformational matrices. Comprised of two ball joints and a prismatic joint, the Orthofix fixator had one redundant DOF that might result in an infinite number of solutions, some of which were valid and represented different final fixator configurations. As revealed by the geometrical and kinematic studies, the extra DOF, which obviously resulted from the rotation of the ball joints, could be eliminated by adding a constraint to it. In this situation, even if the number of equations was equal to that of unknown variables, there still might be multiple solutions because of the nonlinearity of the equations. Theoretically, the iterative numerical method is not guaranteed to find all the solutions. Not all of the randomly selected initial estimates yielded solutions, and only some of the produced solutions were valid. These valid solutions were characterized by the same protruded offset of the telescoping joint. The present study found *Z-X-Z* representation could more reliably predict the reducibility of the malalignment and could be more conveniently used for direct kinematic studies in fixators with ball joints than could *X-Y-Z* representation described by Kim *et al*. (2002), which was better used for fixators having only hinge joints.

With different sequences of joint motion, there were six reduction pathways for each numerical solution because there were three connecting joints in the Orthofix external fixator, which were not sequence dependent. However, the three rotational vectors of the ball joints were sequence dependent. When the reduction pathway follows the sequence of movements

described in the kinematic study (Fig. 4), over-distraction of the soft tissue or collision of the bone fragments during the reduction has been a concern (Kim *et al*., 2002). Fortunately, in practice the reduction does not follow this sequence. With an infinitesimal increase of motion and simultaneous joint movements, the fixator could automatically find a pathway with the least resistance to its final configuration. Therefore, the reduction pathway is actually not a concern. The main goal of the mathematical models is to predict the reducibility of a malalignment, the amount of joint motion needed for the reduction, and the maximal allowable adjustability of the fixators.

In this study, the close form solution done by the geometrical approach verifies the numerical iterative solutions for both direct kinematic and inverse kinematic studies. The equations for the geometrical approach seemed less complex, but they could not be applied to situations with more difficult three-dimensional spatial malalignment. Results of the mechanical experiments were very similar to those obtained with the mathematical approaches, but the values were a little larger because of the laxity of the connecting joints.

According to the mathematical models, the adjustability of the fixator could be increased by increasing the length of the central body (k_1+ k_2), increasing the initial offset of the telescoping joint (L_0), increasing the rotational range of ball joints (a_1 or a_2), and decreasing the pin length (S_x). The range of rotation reached its maximum as the initial offset of the telescoping joint reached a critical level (32.77 mm); however, the adjustability might decrease if the initial offset of the telescoping joint was beyond this critical level. Although this study analyzed only one situation with the bone gap at a level corresponding to the middle of the fixator, in this situation the fixator could achieve its maximal adjustability. These observations imply that, during application of the fixators, to get the maximal adjustability surgeons should place the fixing pins at a distance such that the initial offset of the telescoping joint is as close as possible to the critical level and the fracture gap is positioned at the point corresponding to the middle of the fixator.

The present study has shortcomings. Although only a case of simple malalignment was illustrated to explain the advantages of *Z*-*X*-*Z* representation as compared with *X*-*Y*-*Z* representation for fixators with ball joints, this kinematic chain model can also be applied to other situations with more complex three-dimensional malalignment and other types of external fixators with more complex structures. All of the parameters that may affect the adjustability can be analyzed comprehensively. Although only maximal rotational range of motion was investigated in this study, this rotational motion involving three-dimensional movement of all the connecting joints reflects the overall adjustability of the fixator and can be used for comparison among different designs. This kinematic study, however, investigates only the adjustability and does not consider the possible effects that changing these parameters would have on mechanical properties. Higher adjustability may, in fact, be associated with lower mechanical strength, and a longer offset of the telescoping joint may decrease the fixation stiffness.

V. CONCLUSIONS

The adjustability of external fixators reflects the range of allowable locations of pins and the ease of frame application, two important features of external fixators. The kinematic method described in the present study can accurately quantify the adjustability and should be of value in the design of external fixators and may help surgeons further understand the restraints of fixators and hence perform such placements more precisely and effectively.

NOMENCLATURE

a_1, b_1, r_1	rotation of the lower ball joint about the *X*-, *Y*-, and *Z*-axis
a_2, b_2, r_2	rotation of the upper ball joint about the *X*-, *Y*-, and *Z*-axis
c, s	shorthand for cosine and sine
L_0	initial offset of the telescoping joint
L_p	protruded offset of the telescoping joint
P_x, P_y, P_z	translational vectors about the *X*-, *Y*-, and *Z*-axis
r_1, r_2	rotation of the ball joints about the *Z*-axis in *Z*-*X*-*Z* representation
r_1', r_2'	rotation about the new *Z*-axis in *Z*-*X*-*Z* representation
S_x	distance between the bone fragment and the fixator
S_z	vertical distance between the end of the bone fragment and the ball joint
$\boldsymbol{T}_{(P_x, P_y, P_z)}$	translational matrix of bone fragments
$\boldsymbol{T}_{(X, \theta_x)}$, $\boldsymbol{T}_{(Y, \theta_y)}$, and $\boldsymbol{T}_{(Z, \theta_z)}$	rotational matrices of bone fragments
θ_x, θ_y, θ_z	rotational vectors about the *X*-, *Y*-, and *Z*-axis

REFERENCES

Behrens, F., Johnson, W. D., Koch, T. W., and Kovacevic, N., 1983, "Bending Stiffness of Unilateral and Bilateral Fixator Frames," *Clinical Orthopaedics and Related Research*, Vol. 178, No. 9, pp. 103-110.

Behrens, F., and Searls, K., 1986, "External Fixation of the Tibia," *Journal of Bone and Joint Surgery*, Vol. 68B, No. 2, pp. 246-254.

Bone, L., Stegemann, P., McNamara, K., and Seibel, R., 1993, "External Fixation of Severely Comminuted and Open Tibial Pilon Fractures," *Clinical Orthopaedics and Related Research*, Vol. 292, No. 7, pp. 101-107.

Briggs, B. T., and Chao, E. Y. S., 1982, "The Mechanical Performance of the Standard Hoffmann-Vidal External Fixation Apparatus," *Journal of Bone and Joint Surgery*, Vol. 64A, No. 4, pp. 566-573.

Caja, V. L., Kim, W., Larsson, S., and Chao, E. Y. S., 1995, "Comparison of the Mechanical Performance of Three Types of External Fixators: Linear, Circular and Hybrid," *Clinical Biomechanics*, Vol. 10, No. 8, pp. 401-406.

Caja, V. L., Larsson, S., Kim, W., and Chao, E. Y. S., 1994, "Mechanical Performance of the Monticelli-Spinelli External Fixation System," *Clinical Orthopaedics and Related Research*, Vol. 309, No. 12, pp. 257-266.

Chao, E. Y. S., and Hein, T. J., 1988, "Mechanical Performance of the Standard Orthofix External Fixator," *Orthopedics*, Vol. 11, No. 7, pp. 1057-1069.

Christian, C. A., 1998, "General Principles of Fracture Treatment," *Campbell's Operative Orthopaedics*, Canale, S. T. ed., Mosby-Year Book, Inc., St. Louis, USA, pp. 1993-2041.

Craig, J. J., 1989, *Introduction to Robotics. Mechanics and Control*, 2nd ed., Addison-Wesley, MA, USA, pp. 43-56.

Davis, T. J., Topping, R. E., and Blanco, J. S., 1995, "External Fixation of Pediatric Femoral Fractures," *Clinical Orthopaedics and Related Research*, Vol. 318, No. 9, pp. 191-198.

Fischer, D. A., 1983, "Skeletal Stabilization with a Multiplane External Fixation Device: Design Rational and Preliminary Clinical Experience," *Clinical Orthopaedics and Related Research*, Vol. 180, No. 11, pp. 50-62.

Kim, Y. H., Inoue, N., and Chao, E. Y. S., 2002, "Kinematic Simulation of Fracture Reduction and Bone Deformity Correction Under Unilateral External Fixation," *Journal of Biomechanics*, Vol. 35, No. 8, pp. 1047-1058.

Kummer, F. J., 1992, "Biomechanics of the Ilizarov External Fixator," *Clinical Orthopaedics and Related Research*, Vol. 280, No. 7, pp. 11-22.

Nepola, J. A., 1996, "External Fixation," *Fractures in Adults*, Rockwood *et al*. ed., Lippincott-Raven, PA, USA, pp. 229-259.

Paley, D., Fleming, B., Catagni, M., Kristiansen, T., and Pope, M., 1990, "Mechanical Evaluation of External Fixators Used in Limb Lengthening," *Clinical Orthopaedics and Related Research*, Vol. 250, No. 1, pp. 50-57.

Thakur, A. J., 1997, *The Elements of Fracture fixation*, Churchill Livingstone, New York, USA, pp. 47-176.

APPENDIX

1. The Kinematic Equations in *X-Y-Z* Euler Angle Representation

Element (3,1): $s\theta_x s\theta_z - c\theta_x s\theta_y c\theta_z = (-ca_1 sb_1 cr_1 + sa_1 sr_1) cb_2 cr_2 + (ca_1 sb_1 sr_1 + sa_1 cr_1)(sa_2 sb_2 cr_2 + ca_2 sr_2) + ca_1 cb_1(-ca_2 sb_2 cr_2 + sa_2 sr_2)$; Element (1,2): $-c\theta_y s\theta_z = -cb_1 cr_1 cb_2 sr_2 - cb_1 sr_1(-sa_2 sb_2 sr_2 + ca_2 cr_2) + sb_1(ca_2 sb_2 sr_2 + sa_2 cr_2)$; Element (2,3): $-s\theta_x c\theta_y = (sa_1 sb_1 cr_1 + ca_1 sr_1) sb_2 - (-sa_1 sb_1 sr_1 + ca_1 cr_1) sa_2 cb_2 - sa_1 cb_1 ca_2 cb_2$; Element (1,4): $P_x = -(cb_1 cr_1 cb_2 cr_2 - cb_1 sr_1(sa_2 sb_2 cr_2 + ca_2 sr_2) + sb_1(-ca_2 sb_2 cr_2 + sa_2 sr_2))S_x - (cb_1 cr_1 sb_2 + cb_1 sr_1 sa_2 cb_2 + sb_1 ca_2 cb_2)S_z + sb_1(k_1 + k_2 + L_0 + L_p) + S_x$; Element (2,4): $P_y = -((sa_1 sb_1 cr_1 + ca_1 sr_1) cb_2 cr_2 + (-sa_1 sb_1 sr_1 + ca_1 cr_1)(sa_2 sb_2 cr_2 + ca_2 sr_2) - sa_1 cb_1(-ca_2 sb_2 cr_2 + sa_2 sr_2))S_x - ((sa_1 sb_1 cr_1 + ca_1 sr_1) sb_2 - (-sa_1 sb_1 sr_1 + ca_1 cr_1) sa_2 cb_2 - sa_1 cb_1 ca_2 cb_2)S_z - sa_1 cb_1(k_1 + k_2 + L_0 + L_p)$; Element (3,4): $P_z = -((-ca_1 sb_1 cr_1 + sa_1 sr_1) cb_2 cr_2 + (ca_1 sb_1 sr_1 + sa_1 cr_1)(sa_2 sb_2 cr_2 + ca_2 sr_2) + ca_1 cb_1(-ca_2 sb_2 cr_2 + sa_2 sr_2))S_x - ((-ca_1 sb_1 cr_1 + sa_1 sr_1) sb_2 - (ca_1 sb_1 sr_1 + sa_1 cr_1) sa_2 cb_2 + ca_1 cb_1 ca_2 cb_2)S_z + ca_1 cb_1(k_1 + k_2 + L_0 + L_p) - S_z$

2. The Kinematic Equations in Z-X-Z Euler Angle Representation

Element (3,1): $s\theta_x s\theta_z - c\theta_x s\theta_y c\theta_z = sa_1 sr_1'(cr_2 cr_2' - sr_2 ca_2 sr_2') + sa_1 cr_1'(sr_2 cr_2' + cr_2 ca_2 sr_2') + ca_1 sa_2 sr_2'$; Element (1,2): $-c\theta_y s\theta_z = (cr_1 cr_1' - sr_1 ca_1 sr_1')(-cr_2 sr_2' - sr_2 ca_2 cr_2') + (-cr_1 sr_1' - sr_1 ca_1 cr_1')(-sr_2 sr_2' + cr_2 ca_2 cr_2') + sr_1 sa_1 sa_2 cr_2'$; Element (2,3): $-s\theta_x c\theta_y = (sr_1 cr_1' + cr_1 ca_1 sr_1') sr_2 sa_2 - (-sr_1 sr_1' + cr_1 ca_1 cr_1') cr_2 sa_2 - cr_1 sa_1 ca_2$; Element (1,4): $P_x = -((cr_1 cr_1' - sr_1 ca_1 sr_1')(cr_2 cr_2' - sr_2 ca_2 sr_2') + (-cr_1 sr_1' - sr_1 ca_1 cr_1')(sr_2 cr_2' + cr_2 ca_2 sr_2') + sr_1 sa_1 sa_2 sr_2')S_x - ((cr_1 cr_1' - sr_1 ca_1 sr_1') sr_2 sa_2 - (-cr_1 sr_1' - sr_1 ca_1 cr_1') cr_2 sa_2 + sr_1 sa_1 ca_2)S_z + sr_1 sa_1(k_1 + k_2 + L_0 + L_p) + S_x$; Element (2,4): $P_y = -((sr_1 cr_1' + cr_1 ca_1 sr_1')(cr_2 cr_2' - sr_2 ca_2 sr_2') + (-sr_1 sr_1' + cr_1 ca_1 cr_1')(sr_2 cr_2' + cr_2 ca_2 sr_2') - cr_1 sa_1 sa_2 sr_2')S_x - ((sr_1 cr_1' + cr_1 ca_1 sr_1') sr_2 sa_2 - (-sr_1 sr_1' + cr_1 ca_1 cr_1') cr_2 sa_2 - cr_1 sa_1 ca_2)S_z - cr_1 sa_1(k_1 + k_2 + L_0 + L_p)$; Element (3,4): $P_z = -(sa_1 sr_1'(cr_2 cr_2' - sr_2 ca_2 sr_2') + sa_1 cr_1'(sr_2 cr_2' + cr_2 ca_2 sr_2') + ca_1 sa_2 sr_2')S_x - (sa_1 sr_1' sr_2 sa - sa_1 cr_1' cr_2 sa_2 + ca_1 ca_2)S_z + ca_1(k_1 + k_2 + L_0 + L_p) - S_z$

Manuscript Received: Dec. 22, 2003
Revision Received: Jan. 31, 2004
and Accepted: Mar. 12, 2004